In Operando Photoelectrochemical Femtosecond Transient Absorption Spectroscopy of $WO_3/BiVO_4$ Heterojunctions

Ivan Grigioni,[a] Lucia Ganzer,[b] Franco V.A. Camargo,[b] Benedetto Bozzini,[c] Giulio Cerullo,[b] and Elena Selli*[,a]

[a] Dipartimento di Chimica, Università degli Studi di Milano, Via Golgi 19, I-20133 Milano, Italy

[b] IFN-CNR, Department of Physics, Politecnico di Milano, Piazza Leonardo da Vinci 32, I-20133 Milano, Italy

[c] Department of Innovation Engineering, Università del Salento, via Monteroni s.n., I-73100 Lecce, Italy

ABSTRACT: The $WO_3/BiVO_4$ heterojunction is a promising photoanode architecture for water splitting applications. Here, the photoinduced charge carrier dynamics occurring in this system *in operando* photoelectrochemical conditions, i.e. under an applied anodic potential, are studied through femtosecond transient absorption spectroscopy, to unveil the effects of an applied bias on the early charge carrier dynamics following $WO_3/BiVO_4$ excitation. Electrochromic measurements on $BiVO_4$ suggest the presence of intra band gap (IBG) states in this oxide which play an important role in the charge carrier dynamics in the heterojunction. The differences observed in $WO_3/BiVO_4$ with respect to individual $BiVO_4$ electrodes are rationalized in terms of the electron equilibration between the two oxides at the heterojunction, dominated by the $WO_3/BiVO_4$ interfacial electric field arising from their band energy offset, and the bias-dependent alteration of the IBG states, both determining the rate of hole transfer and accumulation at the $BiVO_4$ surface.

Among n-type metal oxide semiconductors with small band gap (BG), $BiVO_4$ (BG = 2.4 eV) is promising as photoanode material for water splitting, exhibiting good visible-light absorption and a valence band (VB) edge (ca. 2.5 V_{RHE}) suitable for oxygen evolution,[1–7] the limiting reaction in water splitting.[8] However, pure $BiVO_4$ exhibits a rather poor light-to-current conversion efficiency, unless a strongly anodic bias is applied, typically in excess of 1.3 V_{RHE},[9–11] and a limiting photoanodic performance depending on the kinetic competition for long-living photogenerated holes between surface recombination and oxygen evolution, typically occurring in the millisecond to second timescale.[8,12]

Enhanced photoactivity can be obtained by combining smaller and larger BG semiconductor oxides in heterojunctions.[13,14] In particular, in the $WO_3/BiVO_4$ heterojunction (where WO_3 has a BG of 2.7 eV) the two oxides display a staggered (type II) band alignment, the conduction band (CB) minimum and the VB maximum of WO_3 (ca. +0.4 and +3.1 V, respectively) both being lower in energy than those of $BiVO_4$ (ca. +0.02 and +2.4 V, respectively). This allows the injection of electrons photoexcited in $BiVO_4$ into the WO_3 CB, leading to enhanced spatial separation of charges, lower carrier recombination and hole accumulation in $BiVO_4$, while photoexcited electrons rapidly diffuse to the external circuit thanks to their higher mobility in WO_3.[15,16]

Charge carrier dynamics in photoactive materials can be studied through transient absorption (TA) spectroscopy from the picosecond to the second timescale.[8,17–25] In particular, a close-knit group of papers recently appeared on ultrafast (femtosecond to picosecond) TA of $BiVO_4$-related systems, i.e. pure $BiVO_4$,[22,23,26,27] W-doped $BiVO_4$,[28] and the $WO_3/BiVO_4$ heterojunction.[7,15,24,29] However, the charge carrier dynamics has been scarcely investigated so far *in operando* photoelectrochemical (PEC) conditions which are relevant for water splitting applications, i.e. under an applied bias. In their TA studies on pure $BiVO_4$ Ravensbergen et al.[23] observed no spectral or kinetic differences by applying a bias voltage, while a comparison between the TA signals obtained, on the microsecond time scale, with and without applied bias very recently appeared for $BiVO_4$ combined with black phosphorene.[30] Moreover, recent investigations of the $WO_3/BiVO_4$ junction under an applied bias on the long (microsecond to second) timescales relevant to water

oxidation reveal that electron transfer from $BiVO_4$ to WO_3 occurs in the sub-μs time range and that an anodic bias (> 0.6 V_{RHE}) is required to increase the lifetime and population of the holes that oxidize water.[31] Thus, the important effects of an applied bias on the very fast photoinduced dynamics in the $WO_3/BiVO_4$ heterojunction need to be elucidated.

Here we investigate the carrier dynamics in photoexcited $BiVO_4$ and in the $WO_3/BiVO_4$ heterojunction under applied bias in an electrochemical cell, i.e. *in operando* PEC conditions, by combining femtosecond TA spectroscopy with the electrochromic and PEC characterization of the materials.

The photoelectrodes were prepared by spin coating $BiVO_4$ or WO_3 followed by $BiVO_4$ on fluorine doped tin oxide, as previously detailed (see Supporting Information),[7] and consisted of 100 nm thick monoclinic WO_3, 60 nm thick monoclinic scheelite $BiVO_4$ and (100+60) nm thick $WO_3/BiVO_4$ films with high optical quality. Their absorption spectra are shown in Figure 1A. Under an applied potential, WO_3 and $BiVO_4$ photoanodes generate moderate photocurrents, while the $WO_3/BiVO_4$ heterojunction generates larger photocurrents[7,15,16,29,32] (see J-V curves reported in Figure S1), resulting in a higher internal quantum efficiency of the heterojunction[33] in the visible (λ > 400 nm), as shown in Figure 1B.

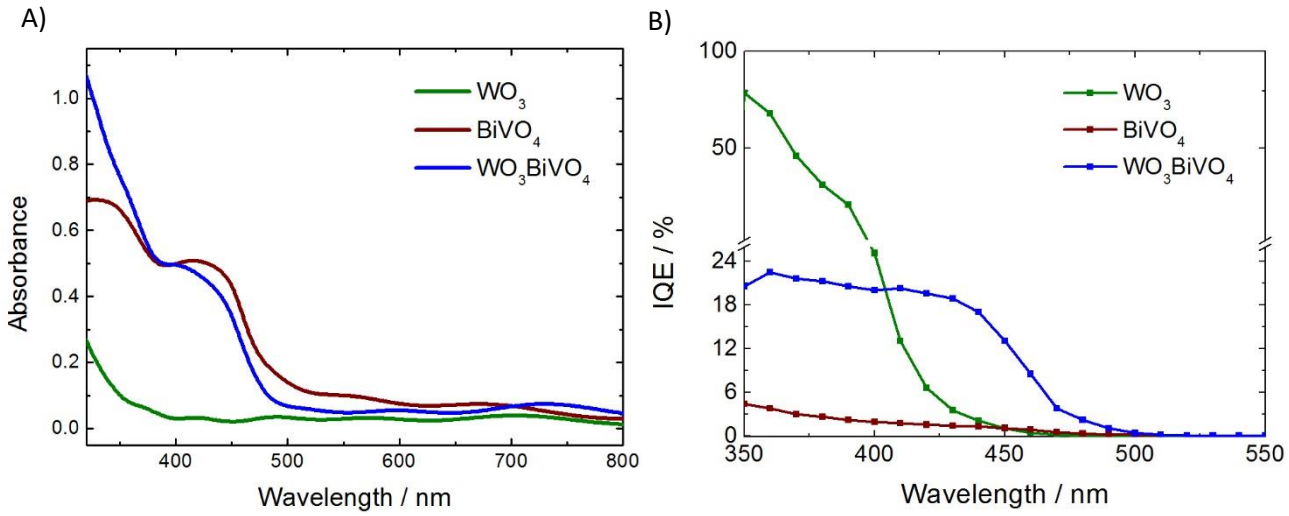

Figure 1. A) Steady-state absorption spectra of the WO_3, $BiVO_4$ and $WO_3/BiVO_4$ electrodes. B) Internal Quantum Efficiency (IQE) as a function of the irradiation wavelength at an applied potential of 1.23 V vs. RHE of the WO_3, $BiVO_4$ and $WO_3/BiVO_4$ photoanodes in 0.5 M Na_2SO_4.

We preliminarily performed spectro-electrochemical experiments by recording the absorption changes induced in $BiVO_4$ and $WO_3/BiVO_4$ by anodic bias at potentials comparable to those used in PEC and *in operando* TA experiments. Steady-state spectra have previously been collected for $BiVO_4$ with an applied bias.[34] The differential absorption (ΔA) spectra of $BiVO_4$ at different potentials, recorded after 60 s applied bias in the electrolyte solution detailed in Section 1.3 of the Supporting Information, are shown in Figure 2A. The spectra were obtained by subtracting the absorption spectrum recorded at the open circuit potential (OCP, i.e. without applied bias) from the absorption spectrum measured at each applied bias in contact with an electrolyte solution.

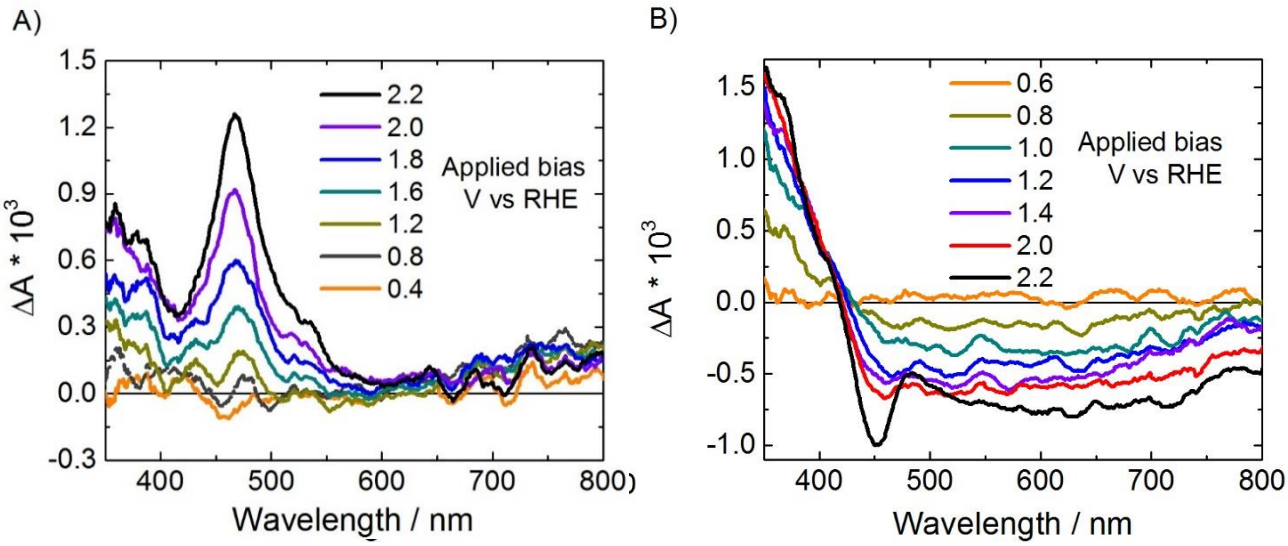

Figure 2. Spectro-electrochromic analyses performed in 0.1 M tetrabutyl ammonium hexafluoro phosphate in acetonitrile solution of A) $BiVO_4$ and B) $WO_3/BiVO_4$ photoanodes, showing the spectral changes occurring under anodic bias. ΔA is the difference between the absorption spectrum at each applied potential and that recorded under open circuit potential conditions.

At low applied potentials (0.4 V) the ΔA signal is close to the measurement baseline, while at biases higher than 0.8 V_{RHE} a well-defined band peaking at 470 nm appears. As the applied potentials are anodic with respect to the flat band potential, which is ~ 0.02 V_{RHE},[7] the appearance of this band indicates that it originates from the oxidized form of intra band gap (IBG) states at energy a few hundred of meV below the CB of $BiVO_4$. In the absence of an electrochemical bias, these IBG states are occupied by electrons, while they are depopulated under the application of an anodic bias, and a new optical transition involving the promotion of electrons from the most

populated VB states (see the density of states of $BiVO_4$ sketched in Scheme 1) to fill IBG states appears peaking at ca. 470 nm (transition β in Scheme 1A), which has been attributed to trapped holes.[7,8,22] At high anodic potentials a positive ΔA band at wavelengths shorter than 400 nm appears, which may be tentatively assigned to surface transformation of $BiVO_4$ into Bi_2O_3 and V_2O_5, both absorbing in this wavelength range,[2] or to a transition to IBG states from VB states at largely positive energy.

On the other hand, the electrochromic tests on the $WO_3/BiVO_4$ system (see Figure 2B) show a progressive absorption decrease in the visible region upon increasing anodic bias, and only at potential larger than 2.0 V_{RHE} the signal of $BiVO_4$ holes appears at 470 nm. Visible light absorption in WO_3 is ascribed to the excitation of electrons trapped at W^{5+} sites to the CB[29,35] (see Scheme 1A). However, at potentials up to 2.0 V - i.e. more positive than WO_3 CB -, no bias-induced absorption change was evidenced with WO_3 in the 300-800 nm range, as shown in Figure S2 of the Supporting Information. This suggests that in the ground state of the heterojunction electrons from $BiVO_4$ are trapped in WO_3 at W^{5+} states and they are depleted under applied bias, as demonstrated by the negative ΔA signal at wavelengths above ca. 450 nm in Figure 2B. For the highest bias voltages, a weak ΔA > 0 band peaked at 470 nm, attributed to hole injection into the IBG states of $BiVO_4$, overlaps to this broad background.

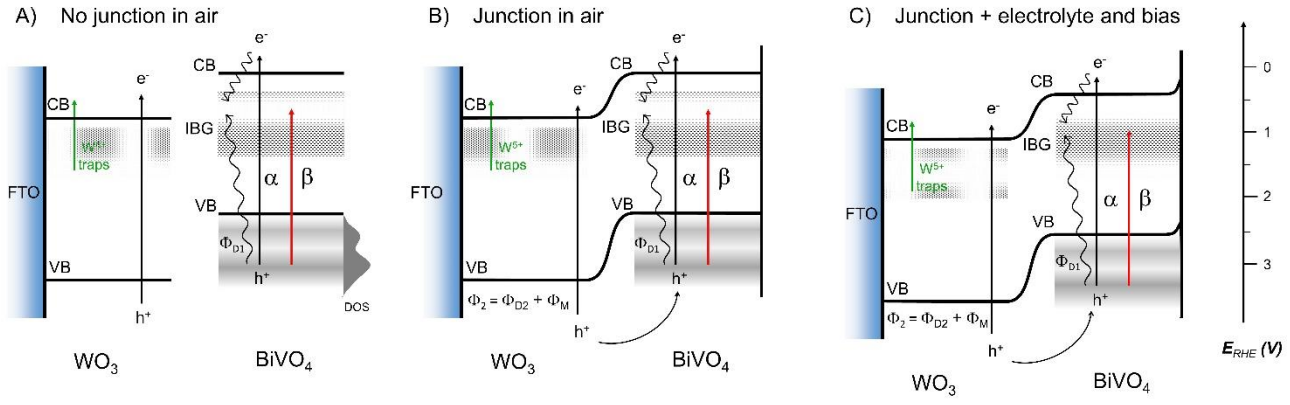

Scheme 1. Scheme of the energy levels and of the transitions occurring A) in separate WO_3 and $BiVO_4$, B) in the $WO_3/BiVO_4$ heterojunction in contact with air, and C) in the $WO_3/BiVO_4$ heterojunction in contact with the electrolyte and under anodic bias. Φ_{D1}: diffusive flux of holes generated by the pump in $BiVO_4$; Φ_2: additional flux of holes in the $WO_3/BiVO_4$ heterojunction, consisting of a diffusive component Φ_{D2} due to

the population imbalance between the VBs of WO_3 and $BiVO_4$, and a migration component Φ_M due to the electric field at the $BiVO_4$ and WO_3 junction.

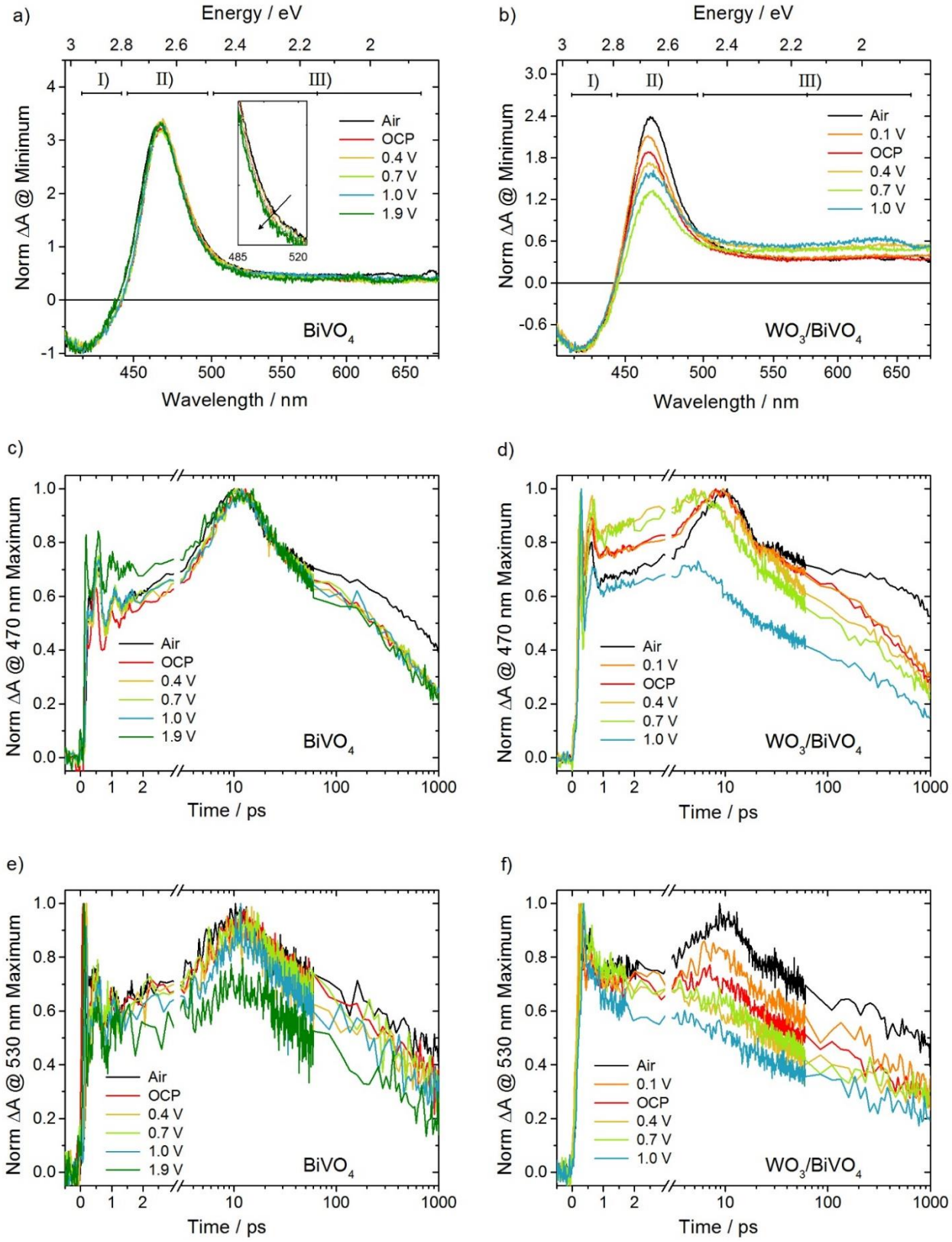

Figure 3. Transient absorption (TA) spectra and time traces measured under applied bias with the electrode in contact with a 0.5 M Na_2SO_4 aqueous solution or with air. (a,b) TA spectra recorded 10 ps after the pump

excitation at 400 nm and normalized with respect to the bleaching maximum for a) $BiVO_4$ and b) $WO_3/BiVO_4$. (c-f) TA dynamics monitored at (c,d) 470 nm and (e,f) 530 nm for (c,e) $BiVO_4$ and (d,f) $WO_3/BiVO_4$, normalized with respect to the signal maximum.

Figures 3a and 3b show the ultrafast TA spectra of $BiVO_4$ and $WO_3/BiVO_4$ films recorded at different applied potentials, as well as at OCP and in air, following excitation by a 100-fs pulse at 400 nm through $BiVO_4$, and probing by a broadband white light continuum. All reported spectra refer to a pump-probe delay of 10 ps and are normalized to the photo bleaching (PB) minimum. Delay dependent TA spectra and TA dynamics at selected wavelengths for $BiVO_4$ and $BiVO_4/WO_3$ at 1 V bias are reported in Figure S3 of the Supporting Information.

The TA signals in both systems essentially originate from $BiVO_4$, since WO_3 films do not show any signal in the relevant time and wavelength range,[7] and can be divided into three regions. As better explained in the Supporting Information, where all dynamics are described in detail, region I) consists in a negative TA signal in the 410-450 nm range (negative band α), implying a decrease of transition α (band gap absorption) in Scheme 1A, and corresponds to PB due to VB depopulation and consequent CB filling resulting in Pauli blocking of the corresponding transitions. The positive TA signal range can be divided into two regions, labeled as II) and III) in Figures 3a and 3b. Region II) covers the 450-530 nm range with the characteristic band peaking at 470 nm (band β) ascribed to transitions from the VB to IBG trapped hole states (transition β in Scheme 1A), while in region III) a broad feature extending to longer wavelengths appears, labeled as band γ, which has been attributed to holes[23] in $BiVO_4$, possibly resulting from intraband transitions within the VB, though also transitions within the CB band or involving IBG states[36] at different energy cannot be excluded. In this region a low intensity tail of band β also persists. Bands α and γ appear instantaneously with the pump pulse, while band β grows within the first tens of picoseconds.

A comparison between Figures 3a and 3b evidences that in $WO_3/BiVO_4$ band β has a lower relative intensity than in $BiVO_4$ (see also Figure S4). This difference can be explained by considering that in the heterojunction electrons have spilled from the IBG states of $BiVO_4$ to the W^{5+} trap states of WO_3 as a consequence of the band alignment (see Scheme 1B) and it is

perfectly in line with the electrochromic tests on $WO_3/BiVO_4$ reported in Figure 2B. In fact, in $WO_3/BiVO_4$ the ground state electron population of the IBG states is lower than in $BiVO_4$. This implies that transition β may occur also in the unperturbed heterojunction, with a consequent decrease of band β intensity in the TA spectra of $WO_3/BiVO_4$ with respect to single $BiVO_4$.

Upon increasing anodic bias, the TA spectrum of $BiVO_4$ displays only minor changes, with a slight contraction on the long wavelengths side of the 470 nm peak (see inset of Figure 3a) and a slight decrease of the γ band (see also Figure S5A). On the other hand, the TA spectrum of $WO_3/BiVO_4$ (Figure 3b) shows a stronger bias-dependence, with the intensity of trapped hole band β decreasing with increasing bias, while band γ increases and tends to become slightly peaked around ca. 650 nm (Figure 3b and Figure S5B). WO_3 contributes to the red portion of the TA spectrum in region III), since reduced WO_3 shows a characteristic absorption feature at wavelengths longer than 550 nm, due to the optical transition involving electrons from W^{5+} states to the WO_3 CB.[29,31] Anodic bias fosters the electron injection from $BiVO_4$ to WO_3 at very short times, with a consequent increase of the TA band γ in region III) with respect to unbiased experiments. It is worth noting that an applied bias at potentials lower than the OCP (i.e. 0.1 V_{RHE}, Figure 3b) produces opposite effects on the TA spectra with respect to bias above the OCP, implying that under such conditions the IBG states have a larger population with respect to OCP conditions.

The TA dynamics at 470 and 530 nm for $BiVO_4$ and $WO_3/BiVO_4$ are shown in panels (c-f) of Figure 3. In $BiVO_4$, the presence of an electrochemical bias does not substantially change the dynamics at 470 nm (Figure 3c) as also evidenced from the Global Analysis (see Table 1 and Figures S6-S7), while it leads to considerable effects at 530 nm (the absorption onset of $BiVO_4$), see Figure 3e, where the spectral component characterized by a build-up (band β) starts to be less significant and the maximum TA is attained during the pump pulse.

On the other hand, an applied bias yields more dramatic effects on the $WO_3/BiVO_4$ heterojunction. Indeed, as shown in Figure 3d, the ΔA maximum at 470 nm occurs earlier at a potential larger than 0.4 V_{RHE} and the buildup almost completely disappears at 1.0 V_{RHE}. This is a consequence of the fact that the hole-trapping component of the TA signal becomes progressively

weaker with increasing applied potential, as evidenced in Figure 3b, so that the TA signal at 470 nm reaches its maximum within the pump pulse. The dynamics in the $WO_3/BiVO_4$ system is even more influenced by bias if it is monitored at 530 nm (Figure 3f), with the ΔA signal always being maximized impulsively under applied bias.

Global Analysis[37,38] was carried out with all datasets, as detailed in the Supporting Information (Figures S6-S9). For both $BiVO_4$ and $WO_3/BiVO_4$ the time-dependent TA spectra exhibit a characteristic sequence of four kinetic components with different time constants (see Figures S10-S12 and Table 1).[23] The first time constant τ_0 is below 0.5 ps and accounts for the impulsive build-up of the TA signal, which cannot be resolved with our experimental setup. For this reason τ_0 values are not reported in Table 1. Time constant τ_1 accounts for the hole trapping process, which results in the characteristic build-up at 470 nm (band β), and in air it is shorter for the heterojunction (2.2 ps) with respect to $BiVO_4$ (3.5 ps). This difference can be explained in terms of electronic structure of the heterojunction system, as shown in Scheme 1. In $BiVO_4$ alone, the dynamics of IBG hole-trapping can be depicted as a diffusive flux Φ_{D1} of the holes generated by the pump from the bulk to surface traps.[22] This flux is purely diffusive when $BiVO_4$ is in contact with air, i.e. in the absence of band-bending. In $WO_3/BiVO_4$ Φ_{D1} is accompanied by a second flux Φ_2 of holes from WO_3, which involves a diffusive component Φ_{D2} within WO_3 and a migration component Φ_M due to the electric field at the interface between $BiVO_4$ and WO_3, resulting from the type-II band alignment. The increased build-up rate of band β in the heterojunction thus arises from the additional flux Φ_2. These results are consistent with previous wavelength-dependent femtosecond TA experiments.[15] Furthermore, as shown in Figure S13, the build-up of the β band is clearly faster in $WO_3/BiVO_4$ only when both oxides are excited (i.e. when holes are also formed in WO_3), whereas it is identical in the two systems upon selective excitation of $BiVO_4$ at 500 nm.

Time constant τ_2 accounts for the recombination between trapped holes and free electrons (see Figure S12B-C) which in $WO_3/BiVO_4$ is slower than in $BiVO_4$ (in air τ_2 is ca. 12 ps for $BiVO_4$ and ca. 15 ps for $WO_3/BiVO_4$). This effect might be explained by the presence of an additional loss channel

for free electrons excited in the CB of $BiVO_4$, which can be injected into the CB of WO_3. This process partially prevents the recombination of free electrons with $BiVO_4$ trapped holes. In fact, the fraction of electrons injected into the CB of WO_3 experiences a longer and thus slower recombination path with $BiVO_4$ holes with respect to the direct recombination between free electrons and holes in $BiVO_4$ alone. As a consequence of the longer τ_2 in the coupled system the disappearance of band β is delayed.

Table 1. Time constants and corresponding confidence intervals estimated from the Global Analysis of TA spectra recorded upon excitation at 400 nm of $BiVO_4$ and $WO_3/BiVO_4$ in air and *in operando* in contact with a Na_2SO_4 0.5 M aqueous solution. Potentials are vs. RHE. For τ_1 the confidence interval (0.1 ps) is determined by the instrumental response function of the system.

$BiVO_4$

Applied potential/V	τ_1/ps	τ_2/ps	τ_3/ps
in air	3.5 ± 0.1	11.9 ± 0.1	835±6.8
OCP (0.23 V)	4.5 ± 0.1	14.6±0.1	512±2.5
0.4	4.8 ± 0.1	13.5±0.12	500±3.0
0.7	4.5 ± 0.1	15.0±0.12	513±3.1
1.0	4.6±0.1	15.3±0.12	510±3.3
1.3	4.3±0.1	17.0±0.13	549±3.9
1.6	4.4±0.1	16.8±0.13	546±4.0
1.9	4.5±0.1	18.2±0.14	643±6.5

$WO_3/BiVO_4$

Applied potential/V	τ_1/ps	τ_2/ps	τ_3/ps
in air	2.2±0.1	15.1±0.1	1340±22
0.1	2.6±0.1	23.7±0.13	608±4.2
OCP (0.3 V)	2.72±0.1	21.4±0.11	484±2.5
0.4	1.84±0.1	29.5±0.17	586±5.6

0.7	1.56±0.1	29.2±0.2	618±10
1.0	1.41±0.1	26.2±0.23	666±11

Finally, time constant τ_3, corresponding to the recombination of trapped holes with thermalized electrons occurring in the nanosecond time scale (τ_3 values in Table 1, with accuracy limited by the maximum available delay of 1500 ps), appears to be almost unaffected by the presence of the WO_3 layer and also by the applied bias, under excitation at 400 nm through the $BiVO_4$ layer.

In operando, i.e. under the application of an anodic bias, the TA spectra of $BiVO_4$ and $WO_3/BiVO_4$ differ considerably both in kinetics and spectral features with respect to those measured in air, i.e. in the absence of band bending at the solid/liquid junction. This is reflected by the time constant values reported in Table 1, obtained from Global Analysis. While time constant τ_1 does not show a clear trend with voltage in $BiVO_4$, it dramatically decreases in the heterojunction, with increasing bias down to ca. 1.41 ps at 1 V_{RHE}, indicating a faster hole accumulation at the $BiVO_4$ surface. The anodic polarisation on the one hand oxidizes the IBG states, thus increasing their hole population; on the other hand, it gives rise to an upwards band bending. In principle, the increase of hole concentration in the IBG and band bending have opposite effects on hole injection to the IBG, but the latter effect is found to dominate, resulting in a higher overall flux, in turn leading to a decrease of τ_1. On the other hand, the recombination time constant τ_2 of trapped holes with free electrons becomes longer with increasing applied bias, both in $BiVO_4$ and in $WO_3/BiVO_4$. The anodic bias, giving rise to an upward band bending (Scheme 1C), tends to withdraw mobile electrons from the $BiVO_4$ CB and a smaller concentration of free electrons in the CB thus results in a lower recombination rate with trapped holes, thus explaining the observed increase of τ_2 with increasing anodic voltage. Finally, the recombination of trapped holes with thermalized electrons, occurring in the nanosecond time scale (τ_3 values in Table 1, with accuracy limited by the maximum available delay of 1500 ps), appears to be almost unaffected by the presence of the WO_3 layer and also by the applied bias.

In conclusion, both spectro-electrochemical and TA measurements performed in the present study provide direct evidence of the spillover of the electrons from the IBG states of $BiVO_4$ to WO_3 when the $WO_3/BiVO_4$ heterojunction is formed. Furthermore, *in operando* PEC TA measurements show that the dynamics of photogenerated charge-carriers in $BiVO_4$ and $WO_3/BiVO_4$ is strongly affected by the application of an external bias, the latter system being more sensitive, as a consequence of the electric field built-in at the $WO_3/BiVO_4$ heterojunction. Indeed, in the heterojunction system the hole trapping rate increases by ca. 50% and the rate of electron-hole recombination almost halves on a relatively short timescale (below 1 ns). This effect is amplified in the presence of the applied anodic bias leading to an accumulation of surface trapped holes beneficial for water oxidation.

Supporting Information

The Supporting Information is available free of charge on the ACS Publication websire at DOI: xxxx. Experimental, preparation of photoelectrodes, photo- and spectro-electrochemical characterization, TA and *in operando* TA spectroscopy, Global Analysis, Comparison of the TA spectra of $BiVO_4$ and $WO_3/BiVO_4$, Global Analysis representative DAS and fittings, TA dynamics in $BiVO_4$, TA experiments upon excitation at different wavelength.

Author Information

Corresponding Author

*elena.selli@unimi.it

ORCID

Ivan Grigioni: 0000-0002-9469-4570

Franco V.A. Camargo: 0000-0001-8312-7899

Benedetto Bozzini: 0000-0002-2725-9157

Giulio Cerullo: 0000-0002-9534-2702

Elena Selli: 0000-0001-8391-7639

ACKNOWLEDGMENTS

I.G. and E.S. gratefully acknowledge financial support from MIUR PRIN 2015K7FZLH. The use of instrumentation purchased through the SmartMatLab project, Fondazione Cariplo grant 2013-1766, is gratefully acknowledged.

REFERENCES

(1) Abdi, F. F.; Han, L.; Smets, A. H. M.; Zeman, M.; Dam, B.; Van de Krol, R. Efficient Solar Water Splitting by Enhanced Charge Separation in a Bismuth Vanadate-Silicon Tandem Photoelectrode. *Nat. Commun.* **2013**, 2195.

(2) Lee, D. K.; Choi, K.-S. Enhancing Long-Term Photostability of $BiVO_4$ Photoanodes for Solar Water Splitting by Tuning Electrolyte Composition. *Nat. Energy* **2017**, *3*, 53-60.

(3) Kim, J. H.; Lee, J. S. Elaborately Modified $BiVO_4$ Photoanodes for Solar Water Splitting. *Adv. Mater.* **2019**, *31*, 1806938.

(4) Kudo, A.; Omori, K.; Kato, H. A Novel Aqueous Process for Preparation of Crystal Form-Controlled and Highly Crystalline $BiVO_4$ Powder from Layered Vanadates at Room Temperature and its Photocatalytic and Photophysical Properties. *J. Am. Chem. Soc.* **1999**, *121*, 11459–11467.

(5) Park, H. S.; Kweon, K. E.; Ye, H.; Paek, E.; Hwang, G. S.; Bard, A. J. Factors in the Metal Doping of $BiVO_4$ for Improved Photoelectrocatalytic Activity as Studied by Scanning Electrochemical Microscopy and First-Principles Density-Functional Calculation. *J. Phys. Chem. C* **2011**, *115*, 17870–17879.

(6) Kim, T. W.; Choi, K.-S. Nanoporous $BiVO_4$ Photoanodes with Dual-Layer Oxygen Evolution Catalysts for Solar Water Splitting. *Science* **2014**, *343*, 990–994.

(7) Grigioni, I.; Stamplecoskie, K. G.; Selli, E.; Kamat, P. V. Dynamics of Photogenerated Charge Carriers in WO_3/$BiVO_4$ Heterojunction Photoanodes. *J. Phys. Chem. C* **2015**, *119*, 20792–20800.

(8) Ma, Y.; Pendlebury, S. R.; Reynal, A.; Le Formal, F.; Durrant, J. R. Dynamics of Photogenerated Holes in Undoped $BiVO_4$ Photoanodes for Solar Water Oxidation. *Chem. Sci.* **2014**, *5*, 2964–2973.

(9) Zhong, D. K.; Choi, S.; Gamelin, D. R. Near-Complete Suppression of Surface Recombination in Solar Photoelectrolysis by "Co-Pi" Catalyst-Modified W:$BiVO_4$. *J. Am. Chem. Soc.* **2011**, *133*, 18370–18377.

(10) Sivula, K. Metal Oxide Photoelectrodes for Solar Fuel Production, Surface Traps, and Catalysis. *J. Phys. Chem. Lett.* **2013**, *4*, 1624–1633.

(11) Ziwritsch, M.; Müller, S.; Hempel, H.; Unold, T.; Abdi, F. F.; Van de Krol, R.; Friedrich, D.; Eichberger, R. Direct Time-Resolved Observation of Carrier Trapping and Polaron Conductivity in $BiVO_4$. *ACS Energy Lett.* **2016**, *1*, 888–894.

(12) Cowan, A. J.; Durrant, J. R. Long-Lived Charge Separated States in Nanostructured Semiconductor Photoelectrodes for the Production of Solar Fuels. *Chem. Soc. Rev.* **2013**, *42*,

2281–2293.

(13) Li, H.; Zhou, Y.; Tu, W.; Ye, J.; Zou, Z. State-of-the-Art Progress in Diverse Heterostructured Photocatalysts toward Promoting Photocatalytic Performance. *Adv. Funct. Mater.* **2015**, *25*, 998–1013.

(14) Moniz, S. J. A.; Shevlin, S. A.; Martin, D. J.; Guo, Z.-X.; Tang, J. Visible-Light Driven Heterojunction Photocatalysts for Water Splitting – A Critical Review. *Energy Environ. Sci.* **2015**, *8*, 731–759.

(15) Grigioni, I.; Stamplecoskie, K. G.; Jara, D. H.; Dozzi, M. V.; Oriana, A.; Cerullo, G.; Kamat, P. V.; Selli, E. Wavelength-Dependent Ultrafast Charge Carrier Separation in the WO_3/$BiVO_4$ Coupled System. *ACS Energy Lett.* **2017**, *2*, 1362–1367.

(16) Hong, S. J.; Lee, S.; Jang, J. S.; Lee, J. S. Heterojunction $BiVO_4$/WO_3 Electrodes for Enhanced Photoactivity of Water Oxidation. *Energy Environ. Sci.* **2011**, *4*, 1781–1787.

(17) Yoshihara, T.; Katoh, R.; Furube, A.; Tamaki, Y.; Murai, M.; Hara, K.; Murata, S.; Arakawa, H.; Tachiya, M. Identification of Reactive Species in Photoexcited Nanocrystalline TiO_2 Films by Wide-Wavelength-Range (400−2500 nm) Transient Absorption Spectroscopy. *J. Phys. Chem. B* **2004**, *108*, 3817–3823.

(18) Tamaki, Y.; Furube, A.; Murai, M.; Hara, K.; Katoh, R.; Tachiya, M. Dynamics of Efficient Electron – Hole Separation in TiO_2 Nanoparticles Revealed by Femtosecond Transient Absorption Spectroscopy under the Weak-Excitation Condition. *Phys. Chem. Chem. Phys.* **2007**, *9*, 1453–1460.

(19) Cowan, A. J.; Tang, J.; Leng, W.; Durrant, J. R.; Klug, D. R. Water Splitting by Nanocrystalline TiO_2 in a Complete Photoelectrochemical Cell Exhibits Efficiencies Limited by Charge Recombination. *J. Phys. Chem. C* **2010**, *114*, 4208–4214.

(20) Pesci, F. M.; Cowan, A. J.; Alexander, B. D.; Durrant, J. R.; Klug, D. R. Charge Carrier Dynamics on Mesoporous WO_3 During Water Splitting. *J. Phys. Chem. Lett.* **2011**, *2*, 1900–1903.

(21) Barroso, M.; Pendlebury, S. R.; Cowan, A. J.; Durrant, J. R. Charge Carrier Trapping, Recombination and Transfer in Hematite (α-Fe_2O_3) Water Splitting Photoanodes. *Chem. Sci.* **2013**, *4*, 2724–2734.

(22) Aiga, N.; Jia, Q.; Watanabe, K.; Kudo, A.; Sugimoto, T.; Matsumoto, Y. Electron–Phonon Coupling Dynamics at Oxygen Evolution Sites of Visible-Light-Driven Photocatalyst: Bismuth Vanadate. *J. Phys. Chem. C* **2013**, *117*, 9881–9886.

(23) Ravensbergen, J.; Abdi, F. F.; Van Santen, J. H.; Frese, R. N.; Dam, B.; Van de Krol, R.; Kennis, J. T. M. Unraveling the Carrier Dynamics of $BiVO_4$: A Femtosecond to Microsecond Transient Absorption Study. *J. Phys. Chem. C* **2014**, *118*, 27793–27800.

(24) Loiudice, A.; Cooper, J. K.; Hess, L. H.; Mattox, T. M.; Sharp, I. D.; Buonsanti, R. Assembly and Photocarrier Dynamics of Heterostructured Nanocomposite Photoanodes from Multicomponent Colloidal Nanocrystals. *Nano Lett.* **2015**, *15*, 7347–7354.

(25) Cristino, V.; Marinello, S.; Molinari, A.; Caramori, S.; Carli, S.; Boaretto, R.; Argazzi, R.; Meda, L.; Bignozzi, C. A. Some Aspects of the Charge Transfer Dynamics in Nanostructured WO_3 Films. *J. Mater. Chem. A* **2016**, *4*, 1–12.

(26) Pattengale, B.; Huang, J. Implicating the Contributions of Surface and Bulk States on Carrier Trapping and Photocurrent Performance of $BiVO_4$ Photoanodes. *Phys. Chem. Chem. Phys.* **2017**, *19*, 6831–6837.

(27) Suzuki, Y.; Murthy, D. H. K.; Matsuzaki, H.; Furube, A.; Wang, Q.; Hisatomi, T.; Domen, K.; Seki, K. Rational Interpretation of Correlated Kinetics of Mobile and Trapped Charge Carriers: Analysis of Ultrafast Carrier Dynamics in $BiVO_4$. *J. Phys. Chem. C* **2017**, *121*, 19044–19052.

(28) Pattengale, B.; Huang, J. The Effect of Mo Doping on Charge Separation Dynamics and Photocurrent Performance of $BiVO_4$ Photoanodes. *Phys. Chem. Chem. Phys.* **2016**, *18*, 32820–32825.

(29) Grigioni, I.; Abdellah, M.; Corti, A.; Dozzi, M. V.; Hammarström, L.; Selli, E. Photoinduced Charge-Transfer Dynamics in $WO_3/BiVO_4$ Photoanodes Probed Through Midinfrared Transient Absorption Spectroscopy. *J. Am. Chem. Soc.* **2018**, *140*, 14042–14045.

(30) Zhang, K.; Jin, B.; Park, C.; Cho, Y.; Song, X.; Zhang, S.; Kim, W.; Zeng, H.; Park, J. H. Black Phosphorene as a Hole Extraction Layer Boosting Solar Water Splitting of Oxygen Evolution Catalysts. *Nat. Commun.* **2019**, *10*, 2001.

(31) Selim, S.; Francàs, L.; García-Tecedor, M.; Corby, S.; Blackman, C.; Gimenez, S.; Durrant, J. R.; Kafizas, A. $WO_3/BiVO_4$: Impact of Charge Separation at the Timescale of Water Oxidation. *Chem. Sci.* **2019**, *10*, 2643–2652.

(32) Grigioni, I.; Corti, A.; Dozzi, M. V.; Selli, E. Photoactivity and Stability of $WO_3/BiVO_4$ Photoanodes: Effects of the Contact Electrolyte and of Ni/Fe Oxyhydroxide Protection. *J. Phys. Chem. C* **2018**, *122*, 13969–13978.

(33) Chen, Z.; Jaramillo, T. F.; Deutsch, T. G.; Kleiman-Shwarsctein, A.; Forman, A. J.; Gaillard, N.; Garland, R.; Takanabe, K.; Heske, C.; Sunkara, M.; et al. Accelerating Materials Development for Photoelectrochemical Hydrogen Production: Standards for Methods, Definitions, and Reporting Protocols. *J. Mater. Res.* **2011**, *25*, 3–16.

(34) Zhang, J.; Luo, W.; Li, W.; Zhao, X.; Xue, G.; Yu, T.; Zhang, C. A Dye-Free Photoelectrochemical Solar Cell Based on $BiVO_4$ with a Long Lifetime of Photogenerated Carriers. *Electrochem. Commun.* **2012**, *22*, 49–52.

(35) Yamase, T. Photo- and Electrochromism of Polyoxometalates and Related Materials. *Chem. Rev.* **1998**, *2665*, 307–325.

(36) Okuno, K.; Kato, H.; Vequizo, J. J. M.; Yamakata, A.; Kobayashi, H.; Kobayashi, M.; Kakihana, M. Expansion of the Photoresponse Window of a $BiVO_4$ Photocatalyst by Doping with Chromium(VI). *RSC Adv.* **2018**, *8*, 38140–38145.

(37) Snellenburg, J. J.; Laptenok, S. P.; Seger, R.; Mullen, K. M.; van Stokkum, I. H. M. Glotaran: A Java-Based Graphical User Interface for the R Package TIMP. *J. Stat. Softw.* **2012**, *49*, 1–22.

(38) van Stokkum, I. H. M.; Larsen, D. S.; van Grondelle, R. Global and Target Analysis of Time-Resolved Spectra. *Biochim. Biophys. Acta* **2004**, *1657*, 82–104.